Electronic Supplementary Material (ESI) for Journal of Materials Chemistry A.

Supporting information

Titanium nitride supported ternary metal phosphides for hydrogen evolution

Jia Zhao[1], Nan Liao[1], Daniel Wun Fung Cheung[1], Jingshan Luo*[1]

[1]*Institute of Photoelectronic Thin Film Devices and Technology, Solar Energy Research Center, Key Laboratory of Photoelectronic Thin Film Devices and Technology of Tianjin, Ministry of Education Engineering Research Center of Thin Film Photoelectronic Technology, Renewable Energy Conversion and Storage Center, Nankai University, 300350 Tianjin, China,*

[2]*Haihe Laboratory of Sustainable Chemical Transformations, 300192 Tianjin, China.*

Email: jingshan.luo@nankai.edu.cn

1. Experimental Section

1.1 Materials and chemicals

The $C_{16}H_{36}O_4Ti$ was purchased from Macklin. Acetone and hydrochloric acid (HCl) were purchased from Tianjin Chemical Reagent Co., Ltd. $Ni(NO_3)_2 \cdot 6\ H_2O$, $Fe(NO_3)_2 \cdot 9\ H_2O$, $Co(NO_3)_2 \cdot 6\ H_2O$ were purchased from Aladdin. All chemicals were used without further purification.

1.2 Synthesis of TiN/CFP

Before the experiments, the carbon fiber paper (CFP) (3×3 cm^2) was pretreated with a plasma cleaning instrument.

First, TiO_2 nanowires were grown on the CFP using a hydrothermal method. The CFP was immersed into a $C_{16}H_{36}O_4Ti$ ethanol solution (achieved by dissolving 0.32 g $C_{16}H_{36}O_4Ti$ into 20.0 mL anhydrous ethanol) and ultrasonicated for 40 min, then annealed in a muffle furnace at 400 °C for 30 minutes, forming the TiO_2 seeds on the surface of the CFP. Next, 15 mL HCl, 15 mL acetone, and 1.5 mL $C_{16}H_{36}O_4Ti$ were added into a Teflon-lined stainless autoclave (50 mL volume), and the CFP coated with TiO_2 seed was dipped into the solution. The hydrothermal

reaction was maintained at a constant temperature of 200 °C for 80 min in an electric oven and then cooled at room temperature. The sample was then sonicated with DI water for 10 min and dried in a vacuum oven at 60 °C for 6 h. This process uniformly covered the entire surface of the CFP with a white film of TiO_2 nanowires. Finally, the samples were annealed in NH_3 at temperatures of 900 °C for 3 h with a heating rate of 3 °C min^{-1} to acquire the TiN/CFP.

1.3 Synthesis of $FeNiCo(OH)_x$/TiN/CFP

The $FeNiCo(OH)_x$ nanosheets were electrodeposited on TiN in a standard three-electrode electrochemical system, where the TiN/CFP, Pt foil, and Ag/AgCl were used as the working, counter, and reference electrode, respectively. The aqueous solution containing 0.1 M $Ni(NO_3)_2$, 0.1 M $Co(NO_3)_2$, and 0.05 M $Fe(NO_3)_3$ was used as the electrodeposition solution. The electrodeposition was carried out for 800 s at a constant cathodic voltage of -1.0 V. After deposition, the obtained electrode was washed several times with deionized water.

1.4 Synthesis of NiFe LDH

The NiFe LDH/Ni foam electrodes were fabricated using a hydrothermal growth method with a slightly modified procedure. Briefly, 0.15 g $Ni(NO_3)_2$, 0.20 g $Fe(NO_3)_3$, and 0.3 g urea were mixed in 36 mL deionized water. After the reagents were dissolved, the solution was poured into a 50 mL autoclave with a piece of Ni foam placed against the wall. The growth was carried out at 120 °C in an electric oven for 6 h. After allowing the autoclave to cool naturally to room temperature, the samples were removed, washed with deionized water, and dried naturally in ambient conditions.

1.5 Transformation of $FeNiCo(OH)_x$/TiN/CFP into $FeNiCoP_x$/TiN/CFP

The $FeNiCo(OH)_x$/TiN/CFP electrodes were transformed into $FeNiCoP_x$/TiN/CFP through a phosphidation process in a tube furnace, and NaH_2PO_2 was used as the phosphorus source. In detail, $FeNiCo(OH)_x$/TiN/CFP electrodes and NaH_2PO_2 powder were put at two separate positions in a tube furnace with NaH_2PO_2 located upstream. Typically, 100 mg of NaH_2PO_2 was used. Subsequently, the sample was heated at 290 °C for 3 h in a static Ar atmosphere, and then naturally cooled to ambient temperature under Ar.

1.6 Material characterizations

A Panalytical (the Netherlands) diffractometer (40kV, 15mA, 600W) was used for X-ray diffractometry (XRD) at room temperature. Scanning electron microscopy (SEM) images were obtained using a JSM-7800F field-emission scanning electron microscope (Jeol, Japan). Transmission electron microscopy (TEM), energy dispersive X-ray spectroscopy (EDS), and high-resolution TEM (HRTEM) were performed using a JEM-2800 microscope (Jeol, Japan). A Thermo Scientific ESCALAB 250Xi (Thermo, USA) Xray photoelectron spectrometer with Al Kα (hv = 1486.6 eV) radiation was used to examine the oxidation states of the transition metals, with the containment carbon peak used to calibrate binding energies. Raman spectrum was conducted on JMS1000 (Edinburgh instruments, laser: 532 nm).

1.7 Electrochemical experiments

All electrochemical measurements were performed using a conventional three-electrode configuration on a CHI 760E electrochemical workstation (CHI Instruments, China). For HER in alkaline conditions, a platinum plate and Hg/ HgO were used as counter and reference electrodes, respectively. The $FeNiCoP_x$/TiN/CFP was used as the working electrode. Linear sweep voltammetry

(LSV) was performed at a rate of 1 mV/s in 1 M KOH. Cyclic voltammetry (CV) was tested from 10 - 50 mV/s in 1 M KOH to calculate the double-layer capacitance (C_{dl}). The electrochemical active surface area (ECSA) was calculated according to the method in the literature.[1] The potential *vs*. Hg/HgO was converted to the potential *vs*. the reversible electrode (RHE) according to the Nernst equation: $E_{RHE} = E_{Hg/HgO} + 0.098 + 0.0592$ pH. All polarization curves were *iR*-corrected.

For HER in acidic conditions, a platinum plate and Ag/AgCl were used as counter and reference electrodes, respectively. The $FeNiCoP_x$/TiN/CFP was used as the working electrode. LSV measurements were performed at the rate of 1 mV/s in 0.5 M H_2SO_4. CV measurements were conducted from 10 - 50 mV/s in 0.5 M H_2SO_4 to calculate the C_{dl}. The potential *vs*. Ag/AgCl was converted to the potential *vs*. the reversible electrode (RHE) according to the Nernst equation: $E_{RHE} = E_{Ag/AgCl} + 0.197 + 0.0592$ pH. All polarization curves were *iR*-corrected.

The AEM cell measurements were performed on a DongHua DH7001 Electrochemical workstation. For overall two-electrode water splitting, TFCNP and NiFe LDH/Ni foam electrodes were used for the hydrogen and oxygen evolution reactions, respectively, and the reaction was characterized by linear sweep voltammetry at a scan rate of 1 mV s^{-1} from 2 - 1.2 V. 6 M KOH solution was used as the electrolyte and the flow was driven by a peristaltic pump. The Fumasep FAAM-15 anion exchange membrane was purchased from SciMaterialsHub. The stability was characterized by chronopotentiometry at a current density of 300 mA cm^{-2} for approximately 100 h.

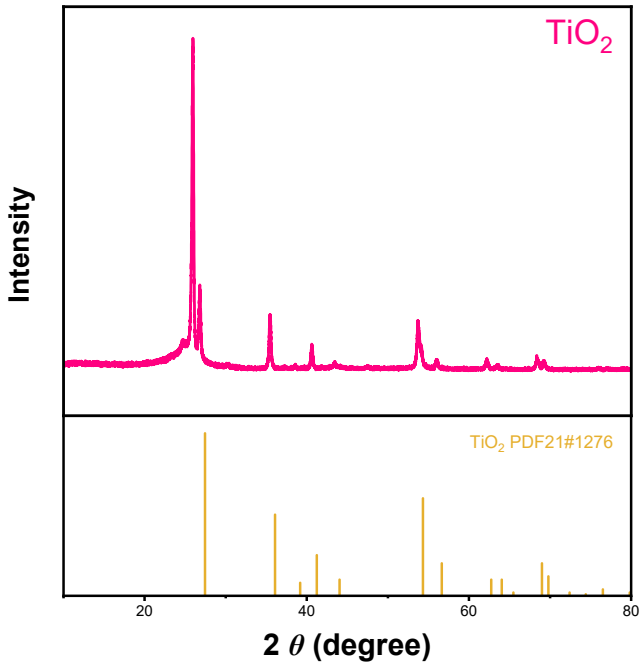

Figure S1. XRD pattern obtained for TiO_2 on CFP.

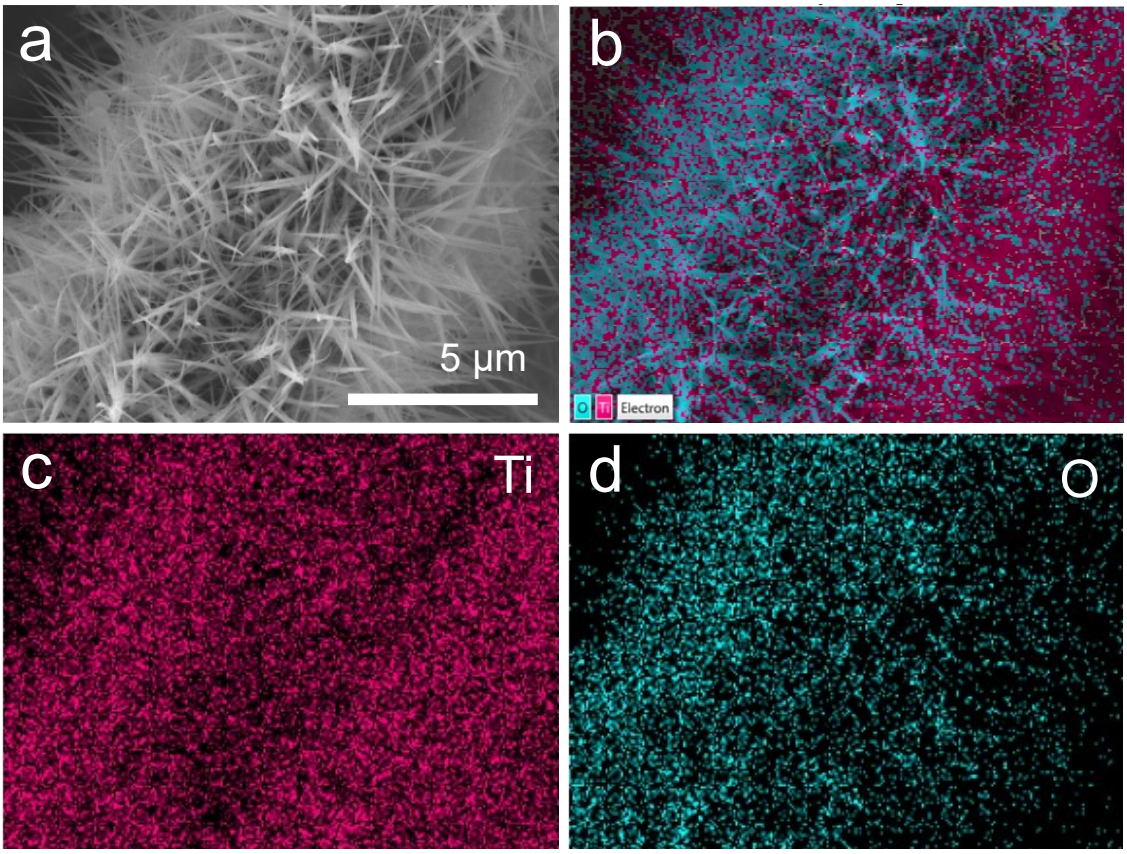

Figure S2. (a) SEM image, **(b-d)** Elemental mapping obtained for TiO_2 on CFP.

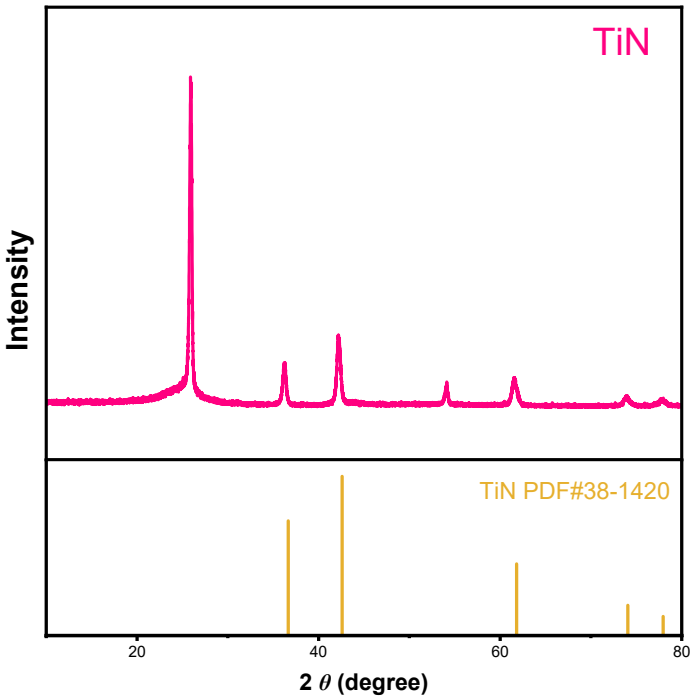

Figure S3. XRD pattern obtained for TiN on CFP.

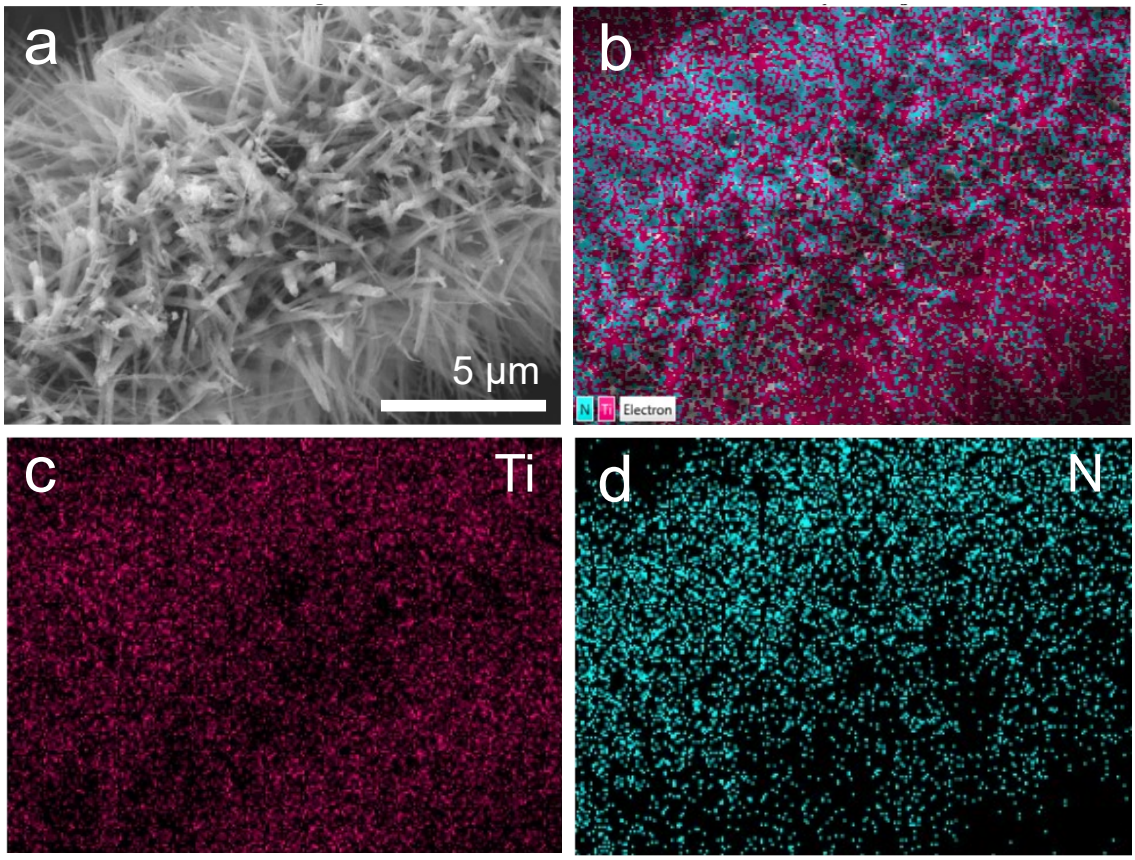

Figure S4. (a) SEM image, **(b-d)** Elemental mapping obtained for TiN on CFP.

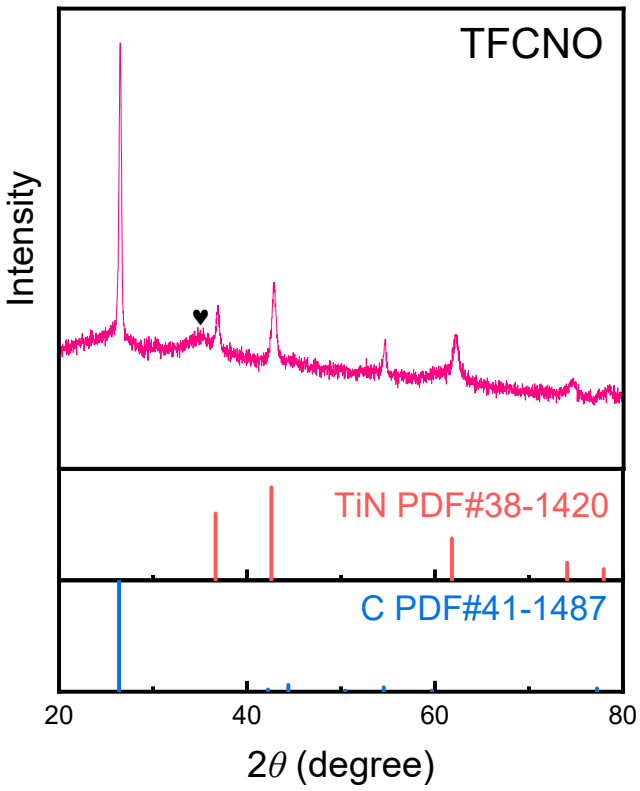

Figure S5. XRD pattern obtained for TFCNO on CFP.

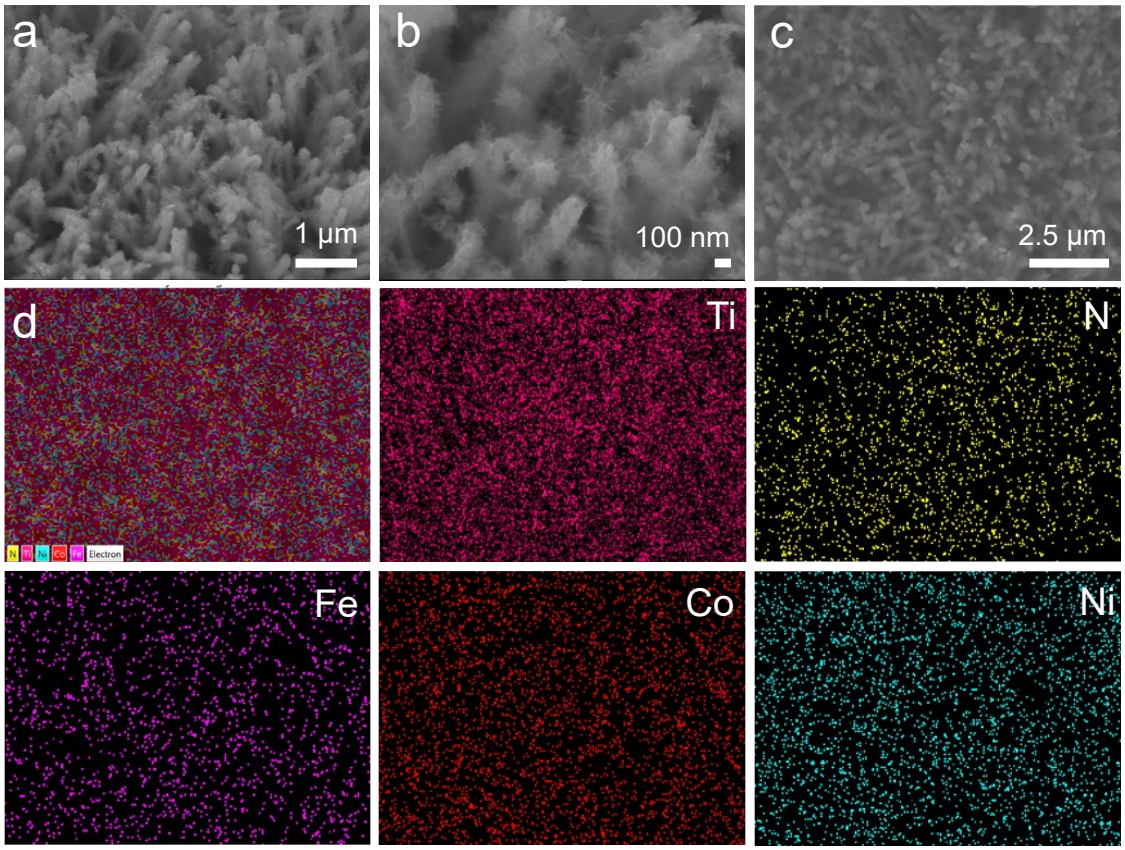

Figure S6. **(a)** Low-magnification, **(b)** high-magnification SEM images, **(c, d)** Elemental mapping obtained for TFCNP.

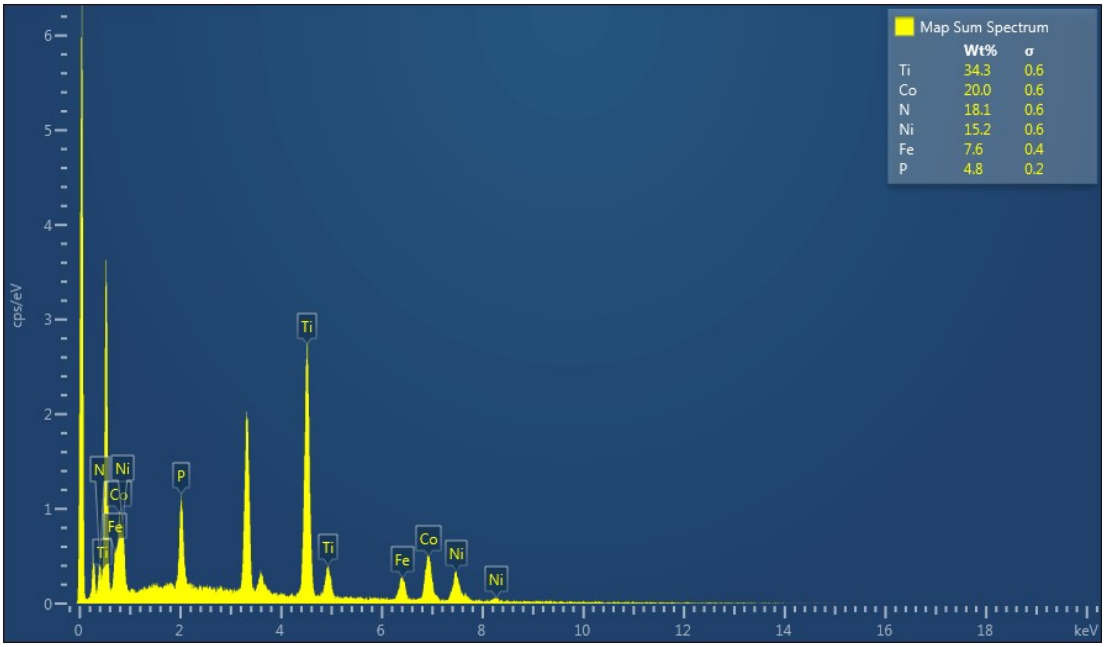

Figure S7. EDX data collected for TFCNO.

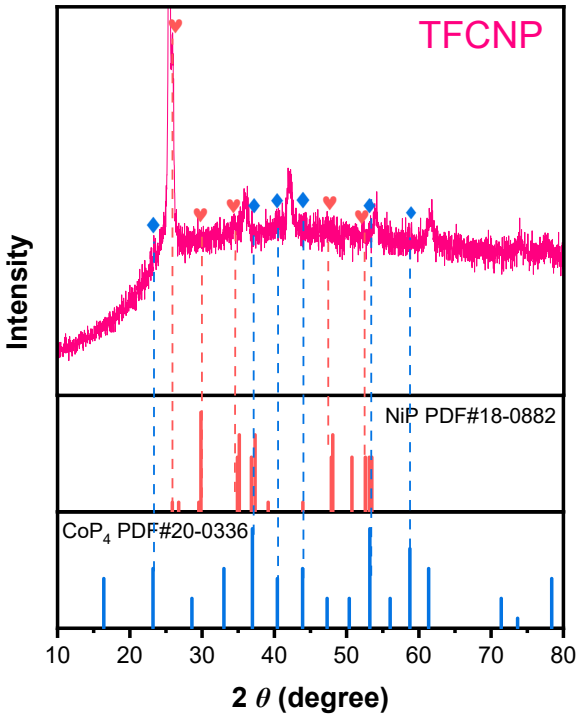

Figure S8. XRD pattern obtained for TFCNP.

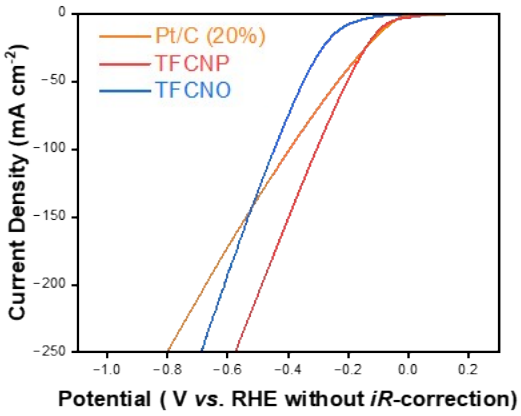

Figure S9. LSV curves measured in 1 M KOH without *iR*-correction.

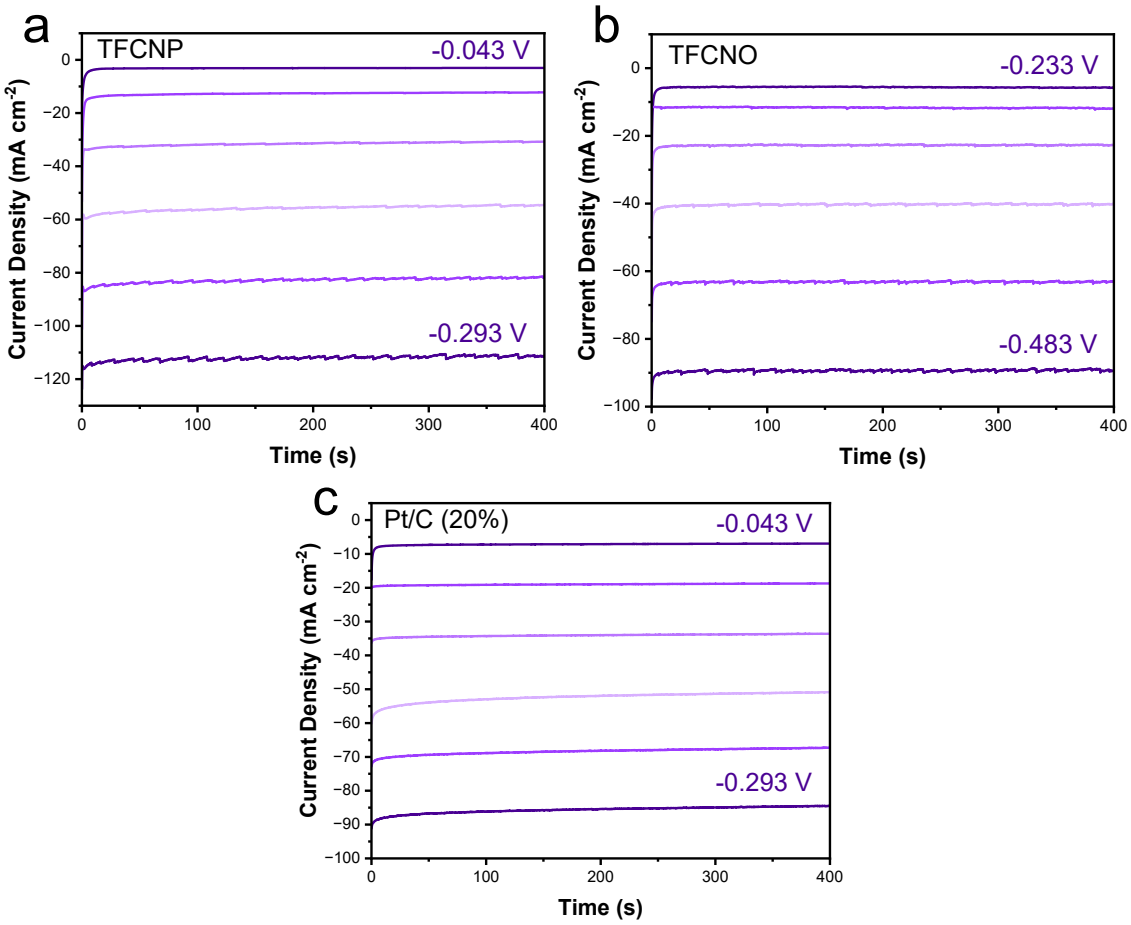

Figure S10. *I-t* curves were measured at different potentials for **(a)** TFCNP, **(b)** TFCNO, and **(c)** Pt/C (20%) during the HER process (1 M KOH).

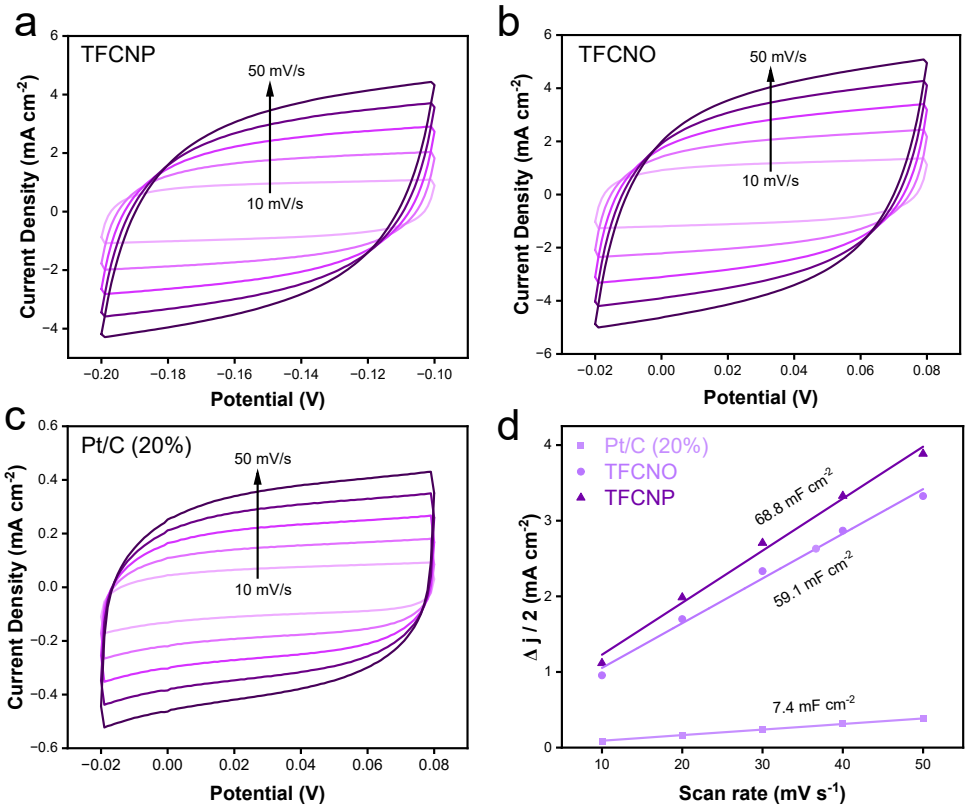

Figure S11. CV curves at different scan rates for **(a)** TFCNP, **(b)** TFCNO, **(c)** Pt/C (20%), **(d)** Current density measured as a function of scan rate (measured in 1 M KOH).

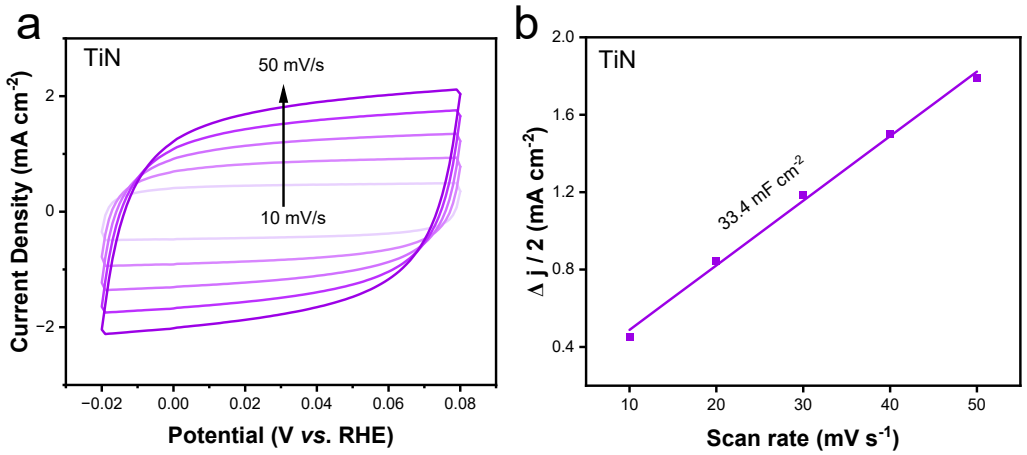

Figure S12. **(a)** CV curves measured for TiN at different scan rates and **(b)** corresponding C_{dl} value (measured in 1 M KOH).

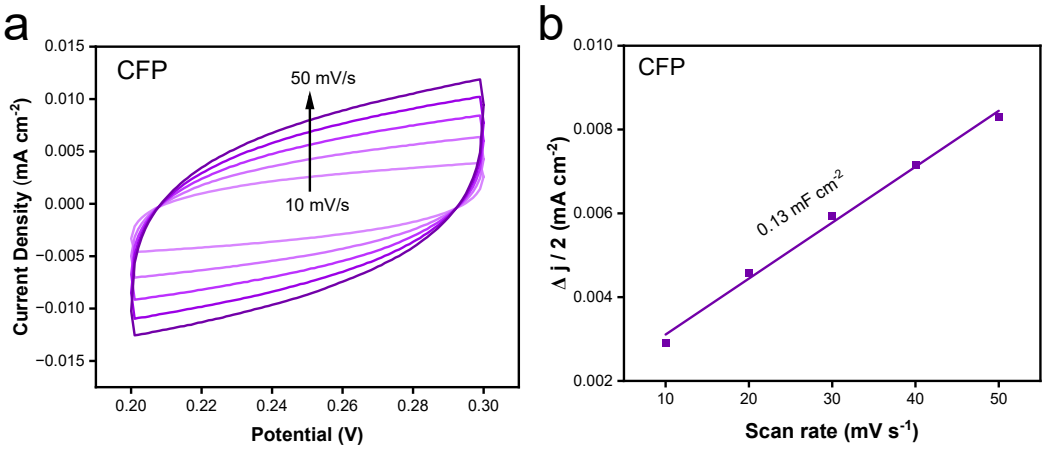

Figure S13. **(a)** CV curves measured for CFP at different scan rates and **(b)** corresponding C_{dl} value (measured in 1 M KOH).

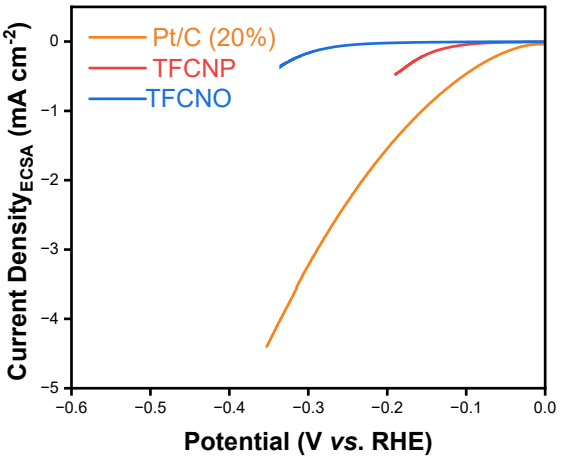

Figure S14. LSV curves normalized to the ECSA in alkaline electrolyte.

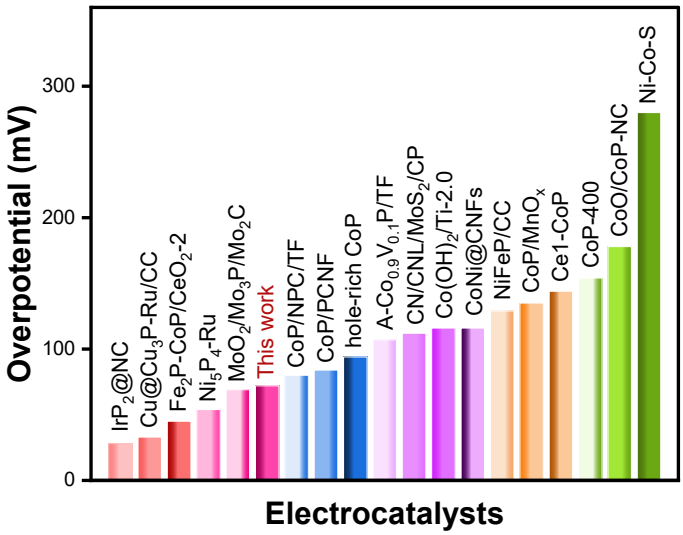

Figure S15. The performance of our TFCNP catalyst compared with reported HER electrocatalysts in terms of overpotential at 10 mA cm^{-2}.

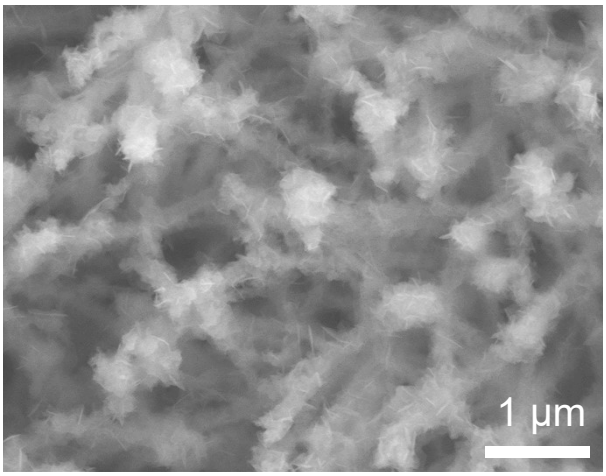

Figure S16. SEM image obtained for TFCNP-S.

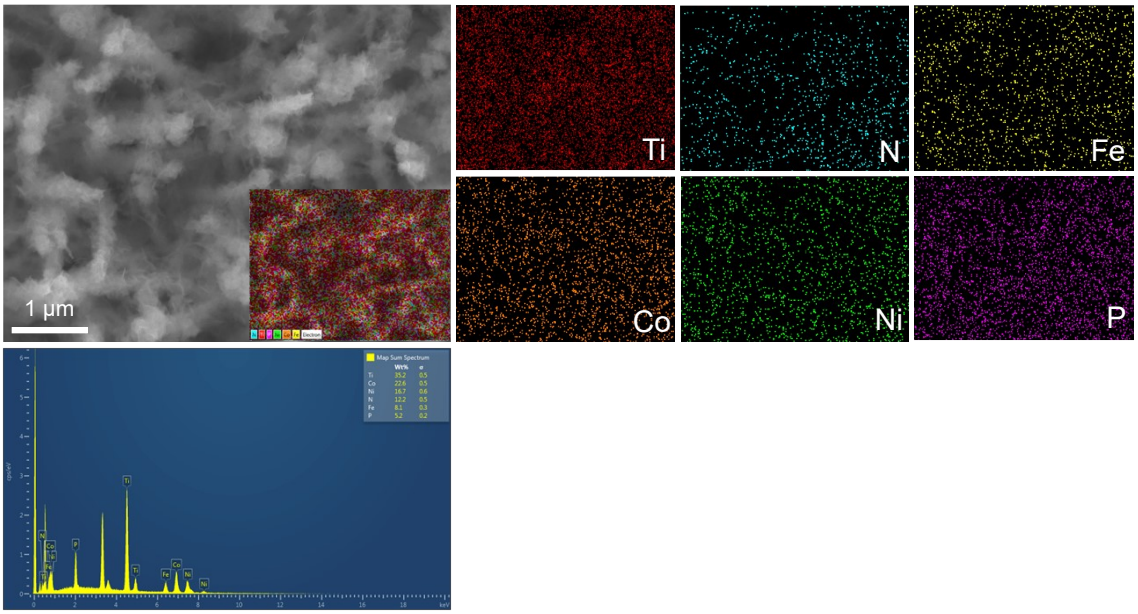

Figure S17. Elemental mapping and EDX spectrum were obtained for TFCNP-S.

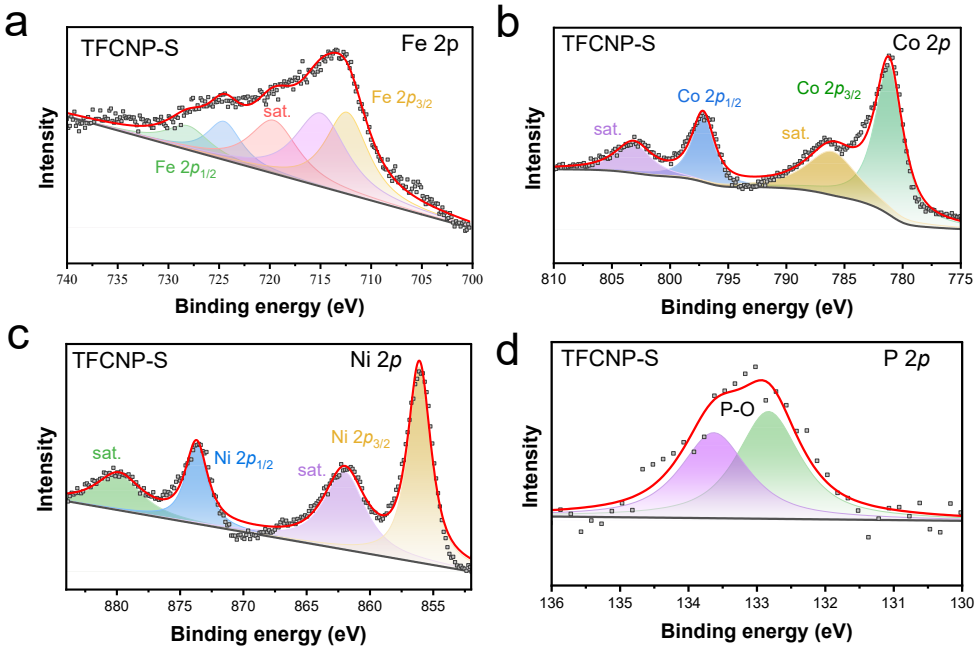

Figure S18. XPS spectra for TFCNP-S.

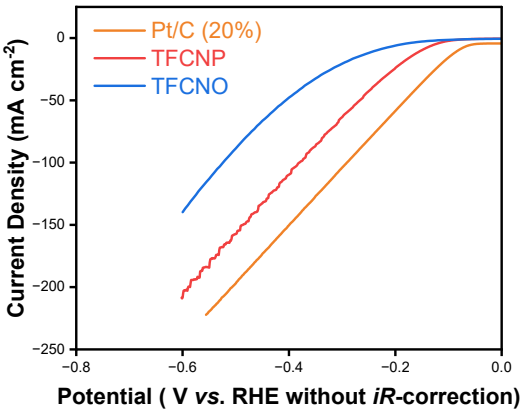

Figure S19. LSV curves measured in 0.5 M H_2SO_4 without *iR*-correction.

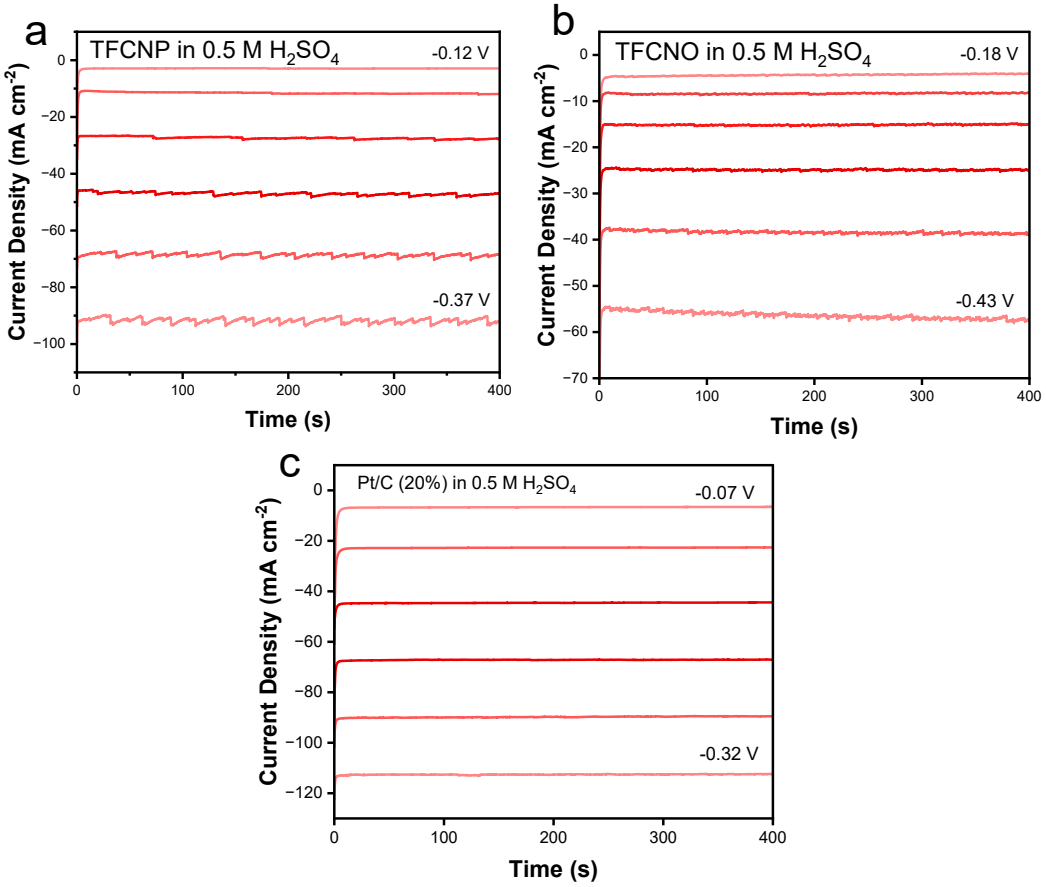

Figure 20. *I-t* curves were measured at different potentials for **(a)** TFCNP, **(b)** TFCNO, and **(c)** Pt/C (20%) during the HER process (0.5 M H_2SO_4).

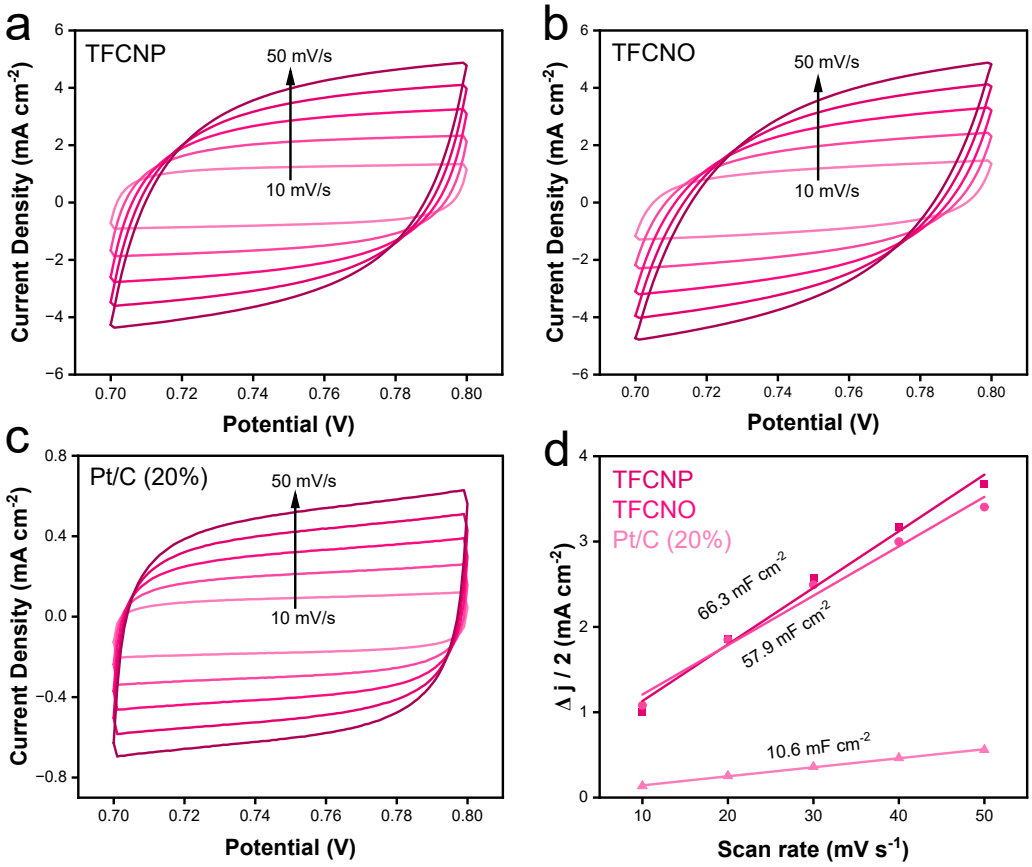

Figure S21. CV curves measured at different scan rates for **(a)** TFCNP, **(b)** TFCNO, **(c)** Pt/C (20%), **(d)** Current density measured as a function of scan rate (measured in 0.5 M H_2SO_4).

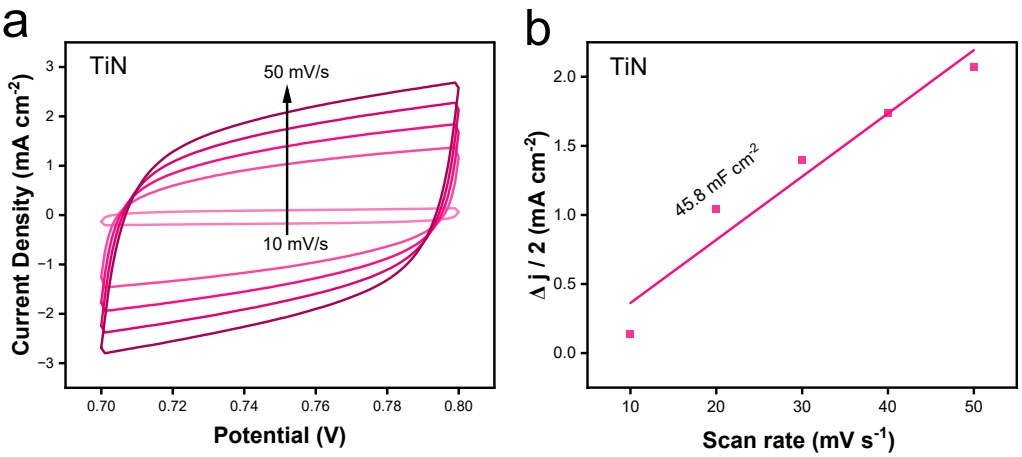

Figure S22. **(a)** CV curves measured for TiN/CFP at different scan rates and **(b)** corresponding C_{dl} value (measured in 0.5 M H_2SO_4).

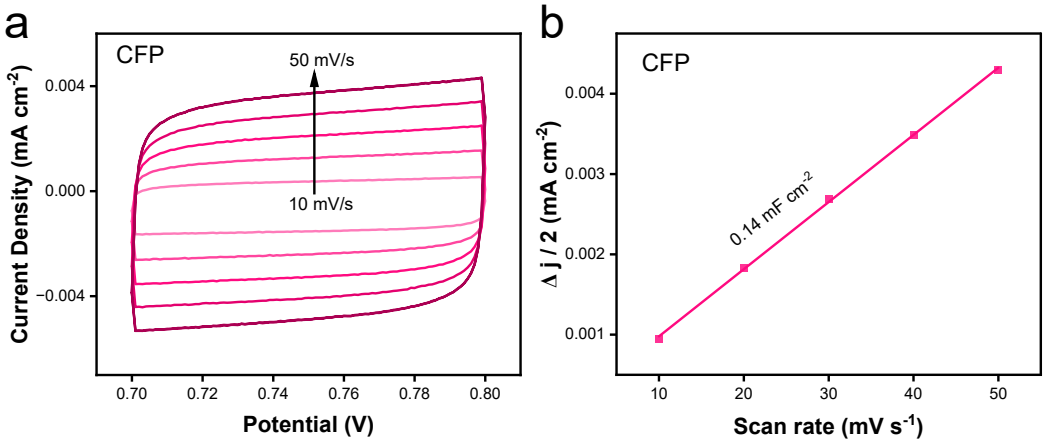

Figure S23. **(a)** CV curves measured for CFP at different scan rates and **(b)** corresponding C_{dl} value (measured in 0.5 M H_2SO_4).

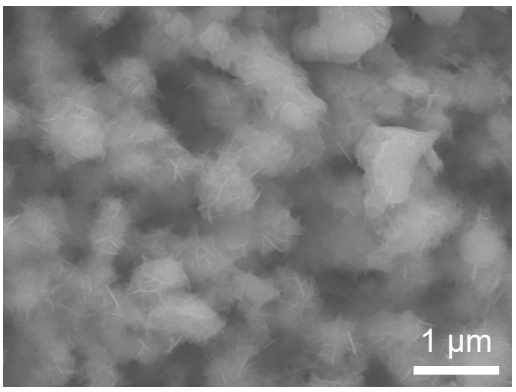

Figure S24. SEM image obtained for TFCNP after HER *i-t* test in 0.5 M H_2SO_4.

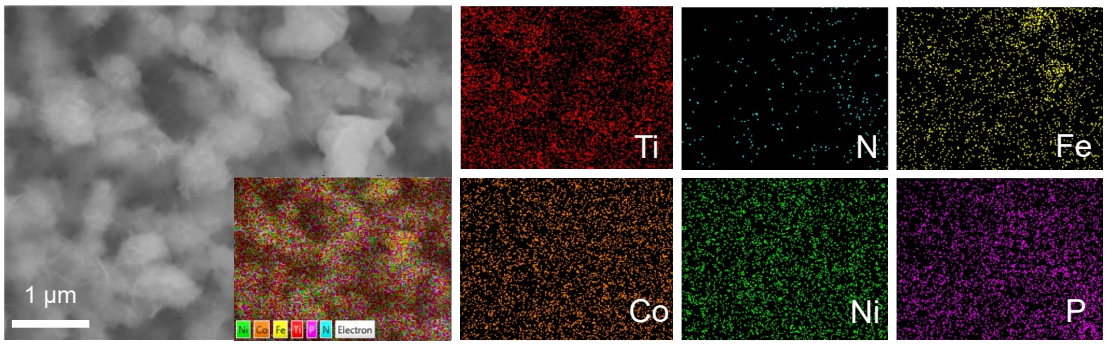

Figure S25. Elemental mapping was obtained for TFCNP after HER *i-t* test in 0.5 M H_2SO_4.

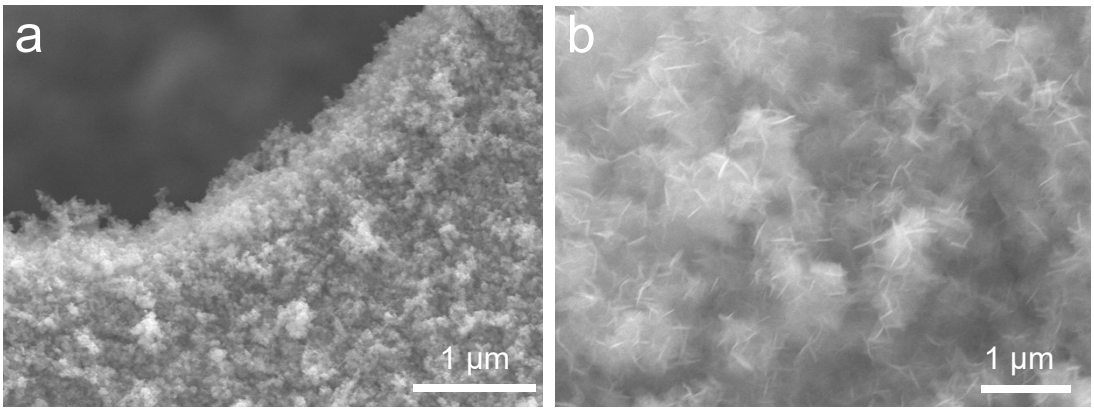

Figure S26. (a) Low and **(b)** High**-** magnification SEM images of NiFe LDH.

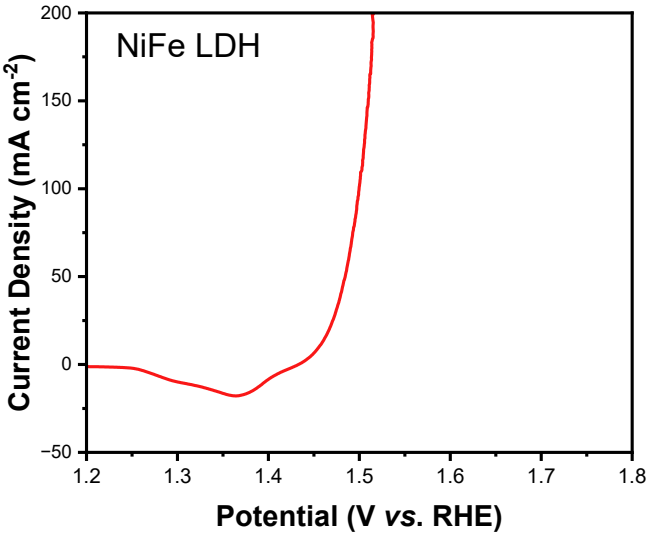

Figure S27. The LSV curve of NiFe LDH.

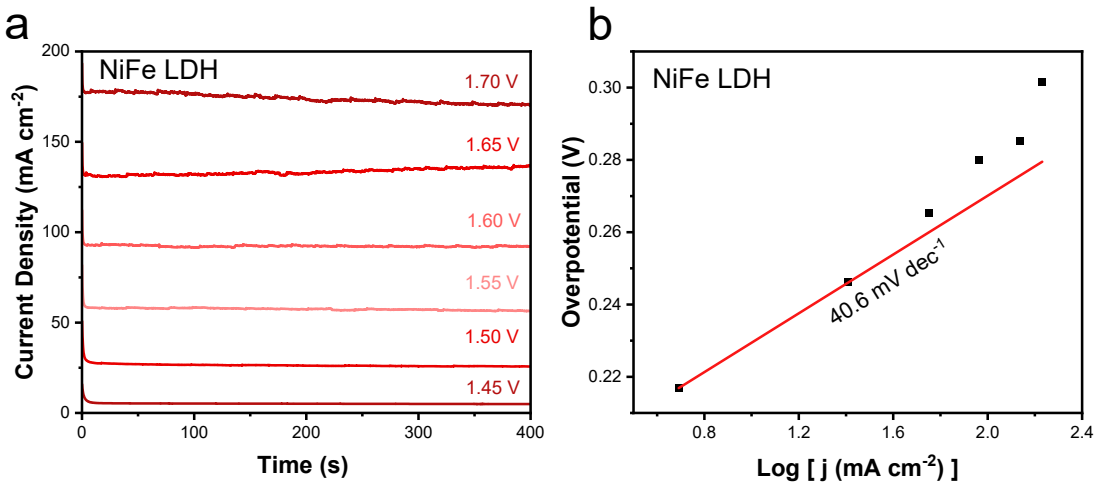

Figure S28. (a) The *i-t* curves at different potentials and **(b)** Tafel slope of NiFe LDH.

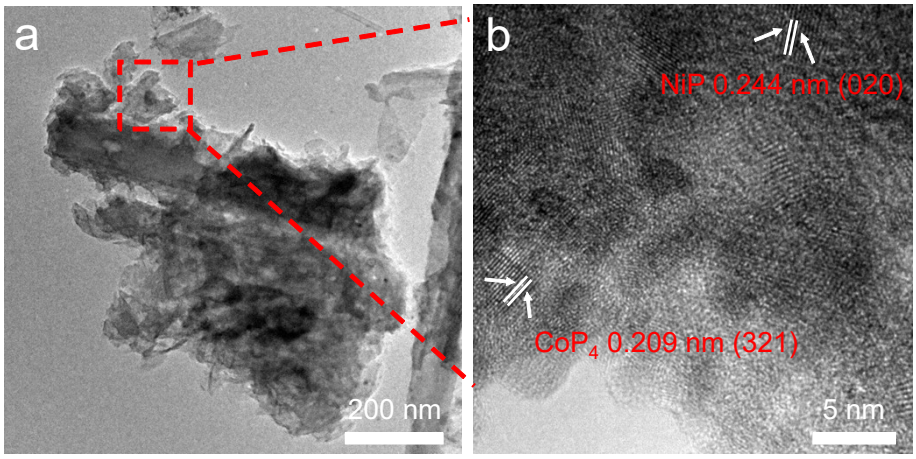

Figure S29. The **(a)** TEM and **(b)** HR-TEM images of TFCNP after the stability test under the industrial condition.

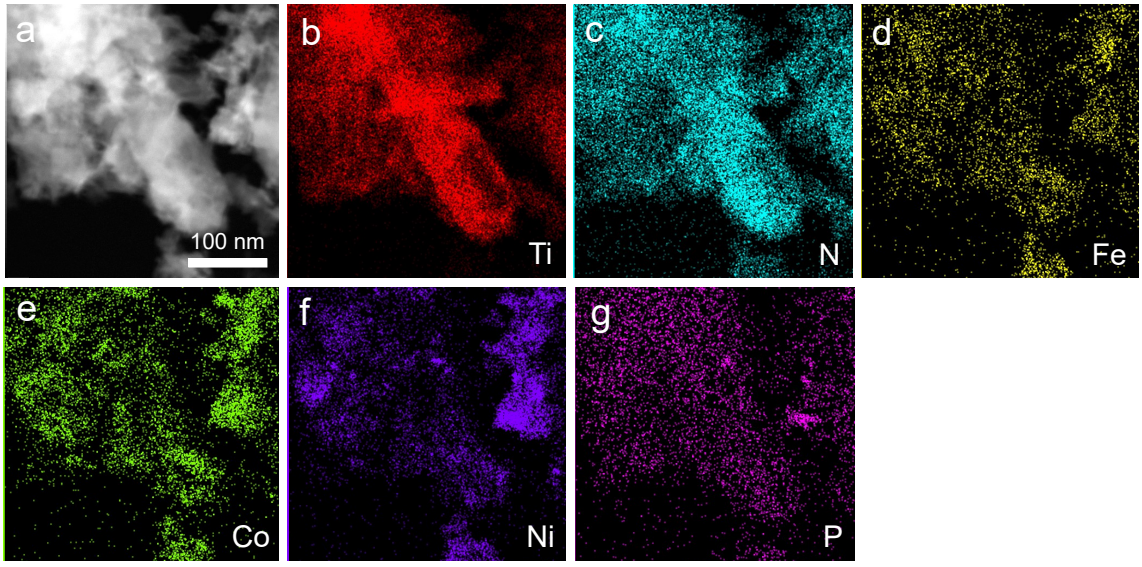

Figure S30. The STEM **(a)** and **(b-g)** the corresponding TEM mapping of TFCNP after the stability test under the industrial condition.

Table S1. Comparison of the electrocatalytic HER performance of the electrode materials reported in this work with recently reported electrocatalysts in the literature.

No	Electrocatalysts	$\eta_{10}(\mathrm{mV})$	electrolyte	Ref.
	TFCNP	72	1 M KOH	This work
1	IrP_2@NC	28	1 M KOH	2
2	Cu@Cu_3P-Ru/CCG	32.97	1 M KOH	3
3	Fe_2P–CoP/CeO_2-20	45	1 M KOH	4
4	Ni_5P_4-Ru	54	1 M KOH	5
5	MoO_2/Mo_3P/Mo_2C	69	1 M KOH	6
6	CoP/NPC/TF	80	1 M KOH	7
7	CoP/PCNF	84	1 M KOH	8
8	Hole-rich CoP	94	1 M KOH	9
9	A-$Co_{0.9}V_{0.1}P$/TF	107	1 M KOH	10
10	CN/CNL/MoS_2/CP	106	1 M KOH	11
11	CoP/Ti-2.0	116	1 M KOH	12
12	CoNi@CNFs	116	1 M KOH	13
13	NiFeP/CC	129	1 M KOH	4
14	CoP/MnO_x	135	1 M KOH	15
15	Ce1−CoP	144	1 M KOH	16
16	Co-400	154	1 M KOH	17
17	CoO/CoP–NC	178	1 M KOH	18
18	Ni−Co−S	280	1 M KOH	19

References

1. Liang, H.; Gandi, A. N.; Anjum, D. H.; Wang, X.; Schwingenschlogl, U.; Alshareef, H. N, *Nano Lett*., 2016, **16**, 7718-7725.
2. Z. Pu, J. Zhao, I. S. Amiinu, W. Li, M. Wang, D. He and S. Mu, *Energy Environ. Sci*., 2019, **12**, 952-957.
3. D. Yang, J.-H. Yang, Y.-P. Yang and Z.-Y. Liu, *App. Catal. B: Environ*., 2023, **326**, 122402.
4. X. Ding, J. Yu, W. Huang, D. Chen, W. Lin and Z. Xie, *Chem. Eng. J*., 2023, **451**, 138550.
5. Q. He, D. Tian, H. Jiang, D. Cao, S. Wei, D. Liu, P. Song, Y. Lin and L. Song, *Adv. Mater*., 2020, **32,** 1906972.
6. J. Xiao, S. Zhang, Y. Sun, X. Liu, G. He, H. Liu, J. Khan, Y. Zhu, Y. Su, S. Wang and L. Han, *Small*, 2023, **19,** 2206472.
7. Huang, X.; Xu, X.; Li, C.; Wu, D.; Cheng, D.; Cao, D, *Adv. Energy Mater*., 2019, **9**, 1803970-1803980.
8. Lu, H.; Fan, W.; Huang, Y.; Liu, T, *Nano Res*., 2018, **11**,1274-1284.
9. Geng, S.; Tian, F.; Li, M.; Guo, X.; Yu, Y.; Yang, W.; Hou, Y, *J. Mater. Chem. A*, 2021, **9**, 8561-8567.
10. Dong, B.; Li, M.-X.; Shang, X.; Zhou, Y.-N.; Hu, W.-H.; Chai, Y.-M, *J. Mater. Chem. A*, 2022, **10**, 17477-17487.
11. Dong, J.; Zhang, X.; Huang, J.; Hu, J.; Chen, Z.; Lai, Y, *Chem. Eng. J*., 2021, **412**, 128556-128565.
12. Yan, Y.; Chen, Y.; Shao, M.; Chen, X.; Yang, Z.; Wang, J.; Chen, H.; Ni, L.; Diao, G, *ACS Sustain. Chem. Eng*., 2023, **11**, 2499-2510.
13. Li, C.; Liu, J.; Gao, R.; Ouyang, H.; Huang, J.; Huang, Q.; Liu, Y, *Int. J. Hydrogen Energy*, 2022, **47**, 34471-34482.
14. Wang, S.; Cai, J.; Lv, C.; Hu, C.; Guan, H.; Wang, J.; Shi, Y.; Song, J.; Watanabe, A.; Ge, X, *Chem. Eng. J*., 2021, **420**, 129972-129984.

15. Yu, R.; Du, Y.-X.; Zhao, H.-F.; Cao, F.-F.; Lu, W.-T.; Zhang, G, *Int*. *J. Hydrogen Energy*, 2023, **48**, 2593-2604.
16. Li, J.; Zou, S.; Liu, X.; Lu, Y.; Dong, D. *ACS Sustain. Chem. Eng*., 2020, **8**, 10009-10016.
17. Li, H.; Zhao, X.; Liu, H.; Chen, S.; Yang, X.; Lv, C.; Zhang, H.; She, X.; Yang, D, *Small*, 2018, **14**, 1802824-2802833.
18. Chen, K.; Cao, Y.; Wang, W.; Diao, J.; Park, J.; Dao, V.; Kim, G.-C.; Qu, Y.; Lee, I.-H, *J. Mater. Chem. A*, 2023, **11**, 3136-3147.
19. Irshad, A.; Munichandraiah, N, *ACS Appl. mater. inter*., 2017, **9**, 19746-19755.